Available online at www.sciencedirect.com

ScienceDirect

Procedia IUTAM 12 (2015) 52 – 61

Procedia IUTAM

www.elsevier.com/locate/procedia

IUTAM Symposium on Mechanics of Soft Active Materials

Computational Modeling of Myocardial Infarction

Ezgi Berberoğlu[a], Serdar Göktepe[a,*]

[a]*Department of Civil Engineering, Middle East Technical University, TR-06800 Ankara, Turkey*

Abstract

Recent developments in computer technology and mathematical modeling have lead to a remarkable improvement in the computational modeling of the cardiovascular system. The virtual heart models have huge potential to understand the electrophysiological and mechanical response of the heart in the healthy and pathological cases. The simulation of physiological behavior of the heart depends on the usage of physiologically sound constitutive models besides the incorporation of the efficient, robust, and stable numerical algorithms. In this contribution, the conservation of linear momentum and excitation equation in the Eulerian setting are solved monolithically through an entirely finite-element based implicit algorithm. The incorporation of the novel generalized Hill model enables us to combine the advantageous features of the active stress and active-strain models. The evolution of the left ventricular pressure is incorporated by a Windkessel-like model. The proposed model is then used to investigate the effect of the myocardial infarction on the pressure-volume curves.

Peer-review under responsibility of Konstantin Volokh and Mahmood Jabareen.

Keywords: Coupled Cardiac Electromechanics, Myocardial Infarction, Pressure-Volume Curves, Finite Element Method

1. Introduction

Heart disease, one of the leading causes of death, is also among the most costly and widespread health problems in the US. Unfortunately, the rate of death related to the cardiac problems is anticipated to increase in the near future[1]. In the case of a cardiac disorder, the cardiovascular system cannot provide the main functionality to maintain the life-sustaining events. One of the most important type of the cardiac dysfunctions is the myocardial infarction (MI) due to its life-threating consequences and the high prevalence[2]. The infarction of the cardiac tissue may decrease the overall efficiency of the heart. Hence, the peripheral tissue and the other organs cannot be supplied with a sufficient amount of blood flow, resulting in a lack of oxygen[3]. Thus, it is of high importance to understand the underlying mechanisms behind the heart function in the healthy and pathological cases to develop novel diagnostic and therapeutic methods.

Among all the non-invasive methods, the pressure-volume (PV) curves are one of the most commonly used clinical tools for the diagnosis of the cardiac disorders. These curves describe the ventricular pressure change with respect to the ventricular volume during a cardiac cycle and are used to measure the mechanical performance and the efficiency

* Serdar Göktepe. Tel.: +90-312-210-2441 ; fax: +90-312-210-5401.
E-mail address: sgoktepe@metu.edu.tr

Peer-review under responsibility of Konstantin Volokh and Mahmood Jabareen.
doi:10.1016/j.piutam.2014.12.007

of the heart[3]. The PV curves are generally preferred for the detection of the cardiac disorders related with the blood flow abnormalities.

The main motivation behind the development of the computational heart models is to come up with new diagnostic and therapeutic tools[4]. In the literature, there are a number of studies on the modeling of the electrophysiological disorders that cover bundle block, arrhythmias and fibrillation[5,6,7,8]. However, there are only few models accounting for the electromechanical disorders where the PV curves are generated from the computational heart models to investigate the ischemia, pulmonary artery construction, and the left bundle block.

The constitutive approaches to the electro-mechanically coupled stress response of the heart can be classified into two groups: the active-strain and active-stress models. In the active-strain based models, the deformation gradient is multiplicatively decomposed into its active and passive parts[9]. The stress response is obtained from a free energy function that is a function of only the elastic part of the deformation gradient. This model has been improved to account for the anisotropic models of cardiac tissue[10,11] and the modeling of smooth muscle contraction[12]. In the active-stress models, however, the stress tensor is additively decomposed into its passive and active components. The passive stress response is a function of only the deformation while the active part depends on the transmembrane potential[13,14,15,16,17,18]. These constitutive approaches have advantages and disadvantages over each other. The active-stress approach is more preferable when the material parameters are identified experimentally in the absence of electrical simulation (passive) and during the active contraction. However, it is generally easier to measure the strain than to measure the local stress fields. In the active-strain approach, it is easier to assess the stability of the material model when the stress tensor is obtained from an energy storage function.

In this contribution, we investigate the effects of myocardial infarction (MI) on PV curves using the computational heart models. The coupled problem of cardiac electromechanics is formulated through the balance of linear momentum and the excitation equation formulated in the Eulerian setting. The recently proposed, novel generalized Hill model[19,20] is utilized to model the electromechanical coupling. In this approach, the advantages of the active-strain and active-stress models are combined. We utilize the two-parameter Aliev-Panfilov model[21] for the simulation of the electrical excitation[22]. The problem of fully coupled cardiac electromechanics is then solved through a unified implicit finite element approach. To model the transient pressure evolution within the ventricles, a Windkessel-based model is incorporated into our model. The proposed model is then used to investigate the effect of MI on the electromechanically coupled behavior of the heart. The computationally obtained PV curves are compared to the clinical findings to assess the capability of our model.

2. Continuous Formulation of Cardiac Electromechanics

In this section, the governing differential equations of the coupled boundary-value problem of cardiac electromechanics are introduced. The electro-mechanical coupling is modeled through the two primary field variables: the placement $\boldsymbol{\varphi}(\mathbf{X}, t)$ depicted in Figure 1 as the deformation map and the transmembrane potential $\Phi(\mathbf{X}, t)$, the difference between the extracellular and intracellular membrane potential[23].

2.1. Kinematics: active-passive decomposition

In Figure 1, the reference configuration $\mathcal{B} \subset \mathbb{R}^3$ and the current configuration $\mathcal{S} \subset \mathbb{R}^3$ of an excitable and deformable solid body are shown. The motion of the material body is described by the non-linear deformation map $\boldsymbol{x} = \boldsymbol{\varphi}_t(\boldsymbol{X}) : \mathcal{B} \to \mathcal{S}$ in the Euclidean space and it maps the material points $\boldsymbol{X} \in \mathcal{B}$ onto their spatial counterparts $\boldsymbol{x} \in \mathcal{S}$. The deformation gradient, $\boldsymbol{F} := \nabla_{\boldsymbol{X}} \boldsymbol{\varphi}_t(\boldsymbol{X}) : T_{\boldsymbol{X}}\mathcal{B} \to T_{\boldsymbol{x}}\mathcal{S}$, is defined as a tangent map between the tangent spaces of the current and reference configurations. Here, $\nabla_{\boldsymbol{X}}[\bullet]$ stands for the gradient operator and denotes the spatial derivative with respect to material coordinates $\boldsymbol{X}$ and the Jacobian $J := \det \boldsymbol{F} > 0$ is the volume map. Referring to[9], the deformation gradient is multiplicatively decomposed into the passive part $\boldsymbol{F}^{\mathrm{e}}$ and the active part $\boldsymbol{F}^{\mathrm{a}}$

$$\boldsymbol{F} = \boldsymbol{F}^{\mathrm{e}} \boldsymbol{F}^{\mathrm{a}} \,. \tag{1}$$

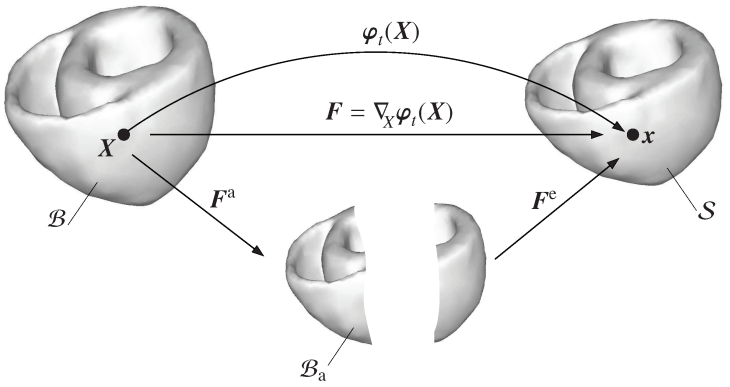

Fig. 1. Motion of an excitable and deformable solid body in the Euclidean space $\mathbb{R}^3$ through the non-linear deformation map $\boldsymbol{\varphi}_t(\boldsymbol{X})$ at time t. The deformation gradient $\boldsymbol{F} = \nabla_X \boldsymbol{\varphi}_t(\boldsymbol{X})$ describes the tangent map between the respective tangent spaces. The deformation gradient $\boldsymbol{F}$ is multiplicatively decomposed into the passive part $\boldsymbol{F}^{\mathrm{e}}$ and the active part $\boldsymbol{F}^{\mathrm{a}}$ with $\mathcal{B}_{\mathrm{a}}$ denoting the fictitious, incompatible intermediate vector space.

Contrary to the total deformation gradient $\boldsymbol{F}$, neither $\boldsymbol{F}^{\mathrm{e}}$ nor $\boldsymbol{F}^{\mathrm{a}}$ can be defined as a gradient of any non-linear deformation map (Figure 1). The active part of the deformation gradient allows us to account for the actively contracting anisotropic architecture of the cardiac tissue through the second-order structural tensors $\boldsymbol{A}_{\mathrm{m}}, \boldsymbol{A}_{\mathrm{n}}$ and $\boldsymbol{A}_{\mathrm{k}}$

$$\boldsymbol{F}^{\mathrm{a}} = \hat{\boldsymbol{F}}^{\mathrm{a}}(\Phi, \boldsymbol{A}_{\mathrm{m}}, \boldsymbol{A}_{\mathrm{n}}, \boldsymbol{A}_{\mathrm{k}})\,. \tag{2}$$

The active part o the deformation gradient for an orthotropic material can be formulated as

$$\boldsymbol{F}^{\mathrm{a}} = \boldsymbol{1} + (\lambda^{\mathrm{a}}_{\mathrm{m}} - 1)\,\boldsymbol{A}_{\mathrm{m}} + (\lambda^{\mathrm{a}}_{\mathrm{n}} - 1)\,\boldsymbol{A}_{\mathrm{n}} + (\lambda^{\mathrm{a}}_{\mathrm{k}} - 1)\,\boldsymbol{A}_{\mathrm{k}} \tag{3}$$

where $\lambda^{\mathrm{a}}_{\alpha} = \hat{\lambda}^{\mathrm{a}}_{\alpha}(\phi)$ for $\alpha = \mathrm{m}, \mathrm{k}, \mathrm{n}$ represent the active stretches in the preferred directions.

2.2. Governing field equations: strong form

The quasi-static mechanical equilibrium is described by the conservation of the linear momentum equation whose local spatial form is given in the form

$$J\,\mathrm{div}[J^{-1}\hat{\boldsymbol{\tau}}] + \boldsymbol{B} = \boldsymbol{0} \quad \text{in} \quad \mathcal{B} \tag{4}$$

where $\hat{\boldsymbol{\tau}}$ is the Eulerian Kirchhoff stress tensor and $\boldsymbol{B}$ is the given body force per reference volume. The operator $\mathrm{div}[\bullet]$ is defined as the divergence with respect to spatial coordinates $\boldsymbol{x}$. The definition of the mechanical problem is completed by introducing the essential (Dirichlet) and natural (Neumann) boundary conditions on the Eulerian surface domain $\partial\mathcal{S}$,

$$\boldsymbol{\varphi} = \bar{\boldsymbol{\varphi}} \quad \text{on } \partial\mathcal{S}_{\varphi} \quad \text{and} \quad \boldsymbol{t} = \bar{\boldsymbol{t}} \quad \text{on } \partial\mathcal{S}_{t}\,. \tag{5}$$

The surface subdomains $\partial\mathcal{S}_{\varphi}$ and $\partial\mathcal{S}_{t}$ satisfy the conditions $\partial\mathcal{S} = \partial\mathcal{S}_{\varphi} \cup \partial\mathcal{S}_{t}$ and $\partial\mathcal{S}_{\varphi} \cap \partial\mathcal{S}_{t} = \emptyset$. The spatial surface traction vector $\bar{\boldsymbol{t}}$ on $\partial\mathcal{S}_{t}$ is defined through the Cauchy stress theorem $\bar{\boldsymbol{t}} := J^{-1}\boldsymbol{\tau} \cdot \boldsymbol{n}$, where $\boldsymbol{n}$ is the outward surface normal defined on $\partial\mathcal{S}$. The other governing differential equation of the coupled problem defines the evolution of the action potential field $\Phi(\boldsymbol{X}, t)$,

$$\dot{\Phi} - J\,\mathrm{div}[J^{-1}\hat{\boldsymbol{q}}] - \hat{I}^{\phi} = 0 \quad \text{in} \quad \mathcal{B} \tag{6}$$

where $\mathrm{div}[J^{-1}\hat{\boldsymbol{q}}]$ is the diffusion term and $\hat{I}^{\phi}$ is the non-linear current source. The material time derivative is denoted by the notation $[\dot{\bullet}] := \mathrm{D}[\bullet]/\mathrm{D}t$. Referring to[24,25], the characteristics of the action potential is controlled by the current source $\hat{I}^{\phi}$ and the recovery variable r, whose evolution equation is introduced in $(13)_2$. Similar to the momentum balance (4), the following essential and natural boundary conditions are introduced for the excitation equation,

$$\Phi = \bar{\Phi} \quad \text{on } \partial\mathcal{S}_{\phi} \quad \text{and} \quad h = \bar{h} \quad \text{on } \partial\mathcal{S}_{h}\,, \tag{7}$$

respectively. The surface subdomain $\partial\mathcal{S}$ satisfies the conditions $\partial\mathcal{S}_\phi \cup \partial\mathcal{S}_h = \partial\mathcal{S}$ and $\partial\mathcal{S}_\phi \cap \partial\mathcal{S}_h = \emptyset$. The electrical surface flux term $\bar{h}$ in $(7)_2$ is formulated through a Cauchy-type formula $\bar{h} := J^{-1}\hat{\boldsymbol{q}}\cdot\boldsymbol{n}$, where $\hat{\boldsymbol{q}}$ is the spatial flux vector. Also, the introduction of an initial condition at $t = t_0$ is necessary due to the term with the material time derivative in the excitation equation (6),

$$\Phi_0(\boldsymbol{X}) = \Phi(\boldsymbol{X}, t_0) \quad \text{in } \mathcal{B}\,. \tag{8}$$

Note that the symbol "hat" used along with the terms $\hat{\boldsymbol{\tau}}$, $\hat{\boldsymbol{q}}$, and $\hat{I}^\phi$ denotes that these variables depend on the primary field variables.

2.3. Constitutive equations

In addition to the two field Equations (4,6) and the corresponding boundary and initial conditions, the solution of the coupled electromechanical problem necessitates the specification of the constitutive equations describing the Kirchhoff stress tensor $\hat{\boldsymbol{\tau}}$, the potential flux $\hat{\boldsymbol{q}}$, and the current source $\hat{I}^\phi$. Following our recently proposed generalized three-dimensional Hill model[19,20], different from the literature[9,26], the free energy function is additively decomposed into the active part $\hat{\Psi}^{\mathrm{a}}$ and the passive part $\hat{\Psi}^{\mathrm{p}}$ [27,28],

$$\Psi = \hat{\Psi}^{\mathrm{p}}(\boldsymbol{g};\boldsymbol{F}) + \hat{\Psi}^{\mathrm{a}}(\boldsymbol{g};\boldsymbol{F}^{\mathrm{e}})\,, \tag{9}$$

where the passive part solely depends on the total deformation gradient and the active part is a function of both the deformation and the potential through the elastic part of the deformation gradient. Decomposition of the free energy function results in a decoupled stress response

$$\boldsymbol{\tau} = \hat{\boldsymbol{\tau}}^{\mathrm{p}}(\boldsymbol{g};\boldsymbol{F}) + \hat{\boldsymbol{\tau}}^{\mathrm{a}}(\boldsymbol{g};\boldsymbol{F}^{\mathrm{e}}) \tag{10}$$

that is obtained by the Doyle-Ericksen formula $\boldsymbol{\tau} := 2\partial_{\boldsymbol{g}}\Psi$ and the elastic part of the deformation gradient is obtained as $\boldsymbol{F}^{\mathrm{e}} = \boldsymbol{F}\boldsymbol{F}^{\mathrm{a}-1}$ from Equation (1). The potential flux $\hat{\boldsymbol{q}}$ is described by the equation,

$$\hat{\boldsymbol{q}} = \hat{\boldsymbol{D}}(\boldsymbol{g};\boldsymbol{F})\cdot\nabla_x\Phi \tag{11}$$

where $\nabla_x\Phi$ and $\hat{\boldsymbol{D}}(\boldsymbol{g};\boldsymbol{F})$ denote the spatial potential gradient and the conduction tensor, respectively. The electrical source term of the Fitzhugh-Nagumo-type excitation equation (6) depends solely on the electrical field

$$\hat{I}^\phi = \hat{I}^\phi(\Phi, r)\,, \tag{12}$$

meaning that the mechano-electrical coupling (deformation-induced current generation) is not taken into account[15,20]. Note that $\hat{I}^\phi$ depends on the recovery variable r as that characterizes the repolarization response of the action potential. The evolution of the recovery variable controls the local shape and duration of the action potential and may vary throughout the heart, therefore, it is modeled by a local ordinary differential equation $(13)_2$. In our formulation, the recovery variable r is treated as an internal history variable that preserves the modular global structure of the field equations (4,6).

3. Specific Constitutive Equations

This section is concerned with the specific constitutive model describing the current source $\hat{I}^\phi$ (12), the Kirchhoff stress tensor $\hat{\boldsymbol{\tau}}$ (10), the evolution of the active part of the deformation gradient $\boldsymbol{F}^{\mathrm{a}}$ (2), the potential flux $\hat{\boldsymbol{q}}$ (11), and the left and right ventricular pressures $(p_{\mathrm{lv}}, p_{\mathrm{rv}})$ as natural boundary conditions $(5)_2$ of the mechanical problem.

3.1. Current source

In this study, the Aliev-Panfilov model, a two-variable phenomenological model[21], is utilized. The local representation of this class of models involves two ordinary differential equations describing the rapidly evolving dimensionless

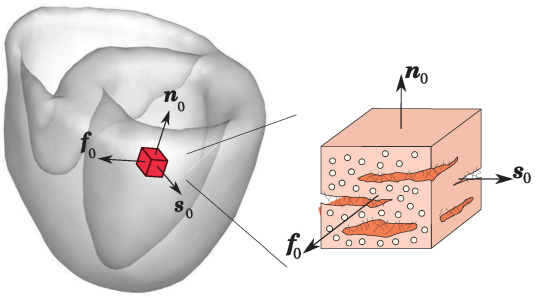

Fig. 2. Anisotropic architecture of the myocardium. The orthogonal unit vectors f_0 and s_0 designate the preferred fiber and sheet directions in the undeformed configuration, respectively. The third direction n_0 is orthogonal to the latter by its definition $n_0 := (f_0 \times s_0)/|f_0 \times s_0|$.

transmembrane potential $\partial_\tau \phi = \hat{i}^\phi(\phi, r)$ and the slowly evolving recovery variable $\partial_\tau r = \hat{i}^r(\phi, r)$. The local ordinary differential equations for the Aliev-Panfilov model are given as

$$\begin{aligned} \partial_\tau \phi &= \hat{i}^\phi(\phi, r) = c\,\phi\,(\phi - \alpha)(1 - \phi) - r\,\phi\,, \\ \partial_\tau r &= \hat{i}^r(\phi, r) = \hat{\epsilon}(\phi, r)\,[-r - c\,\phi\,(\phi - b - 1)]\,, \end{aligned} \tag{13}$$

where α, b, and c are the material parameters and $\hat{\epsilon}(\phi, r) := \gamma + \mu_1 r/(\mu_2 + \phi)$ is the coefficient function controlling the restitution characteristics of the model through the material parameters γ, μ_1, and μ_2 [21,22]. In our formulation [29], we have introduced the dimensionless transmembrane potential ϕ and the dimensionless time τ in (13), related to their physical counterparts through the equations

$$\Phi = \beta_\phi \phi - \delta_\phi \quad \text{and} \quad t = \beta_t \tau\,. \tag{14}$$

3.2. Passive stress response

For the passive response of the myocardium (9), the orthotropic hyperelasticity model [30] is utilized. The free energy function given below is used to express the passive stress response through the volumetric part $U(J)$ and the orthotropic part $\tilde{\Psi}(I_1, I_{4\mathrm{m}}, I_{4\mathrm{n}}, I_{4\mathrm{k}})$

$$\hat{\Psi}^{\mathrm{p}}(\boldsymbol{g}; \boldsymbol{F}) = U(J) + \tilde{\Psi}(I_1, I_{4\mathrm{m}}, I_{4\mathrm{n}}, I_{4\mathrm{k}}) \tag{15}$$

where

$$\tilde{\Psi} = \frac{a_1}{2b_1} \exp[b(I_1 - 3)] + \sum_{i=\mathrm{m,n}} \frac{a_i}{2b_i} \{\exp[b_i (I_{4i} - 1)^2] - 1\} + \frac{a_{\mathrm{k}}}{2b_{\mathrm{k}}} [\exp(b_{\mathrm{k}} I_{4\mathrm{k}}^2) - 1]\,, \tag{16}$$

expressed in terms of the material parameters $a_1, b_1, b_{\mathrm{m}}, a_{\mathrm{n}}, b_{\mathrm{n}}, a_{\mathrm{k}}, b_{\mathrm{k}}$ and the invariants

$$I_1 := \boldsymbol{g} : \boldsymbol{b}\,,\; I_{4\mathrm{m}} := \boldsymbol{g} : \boldsymbol{m}\,,\; I_{4\mathrm{n}} := \boldsymbol{g} : \boldsymbol{n}\,, \quad \text{and} \quad I_{4\mathrm{k}} := \boldsymbol{g} : \boldsymbol{k}\,. \tag{17}$$

Here, the Eulerian structural tensors $\boldsymbol{m}, \boldsymbol{n}$, and $\boldsymbol{k}$ are related to their Lagrangean counterparts through the push-forward relation

$$\boldsymbol{m} := \boldsymbol{F}\boldsymbol{M}\boldsymbol{F}^T\,,\; \boldsymbol{n} := \boldsymbol{F}\boldsymbol{N}\boldsymbol{F}^T\,, \quad \text{and} \quad \boldsymbol{k} := \boldsymbol{F}\boldsymbol{K}\boldsymbol{F}^T. \tag{18}$$

The Lagrangean structural tensors

$$\boldsymbol{M} := \boldsymbol{f}_0 \otimes \boldsymbol{f}_0\,,\; \boldsymbol{N} := \boldsymbol{s}_0 \otimes \boldsymbol{s}_0\,, \quad \text{and} \quad \boldsymbol{K} := \mathrm{sym}(\boldsymbol{f}_0 \otimes \boldsymbol{s}_0) \tag{19}$$

depend on the preferred fiber $\boldsymbol{f}_0$ and sheet directions $\boldsymbol{s}_0$ accounting for the orthotropic microstructure of the myocardium (Figure 2). The passive Kirchhoff stress tensor can be obtained through the Doyle-Ericksen formula

$$\tilde{\boldsymbol{\tau}}^{\mathrm{p}}(\boldsymbol{g};\boldsymbol{F}) = 2\Psi_1\,\boldsymbol{b} + 2\Psi_{4\mathrm{m}}\,\boldsymbol{m} + 2\Psi_{4\mathrm{n}}\,\boldsymbol{n} + 2\Psi_{4\mathrm{k}}\,\boldsymbol{k} \tag{20}$$

in terms of the derivatives of the free energy function with respect to the invariants, the left Cauchy-Green tensor $\boldsymbol{b} := \boldsymbol{F}\boldsymbol{G}^{-1}\boldsymbol{F}^{T}$, and the Eulerian structural tensors.

3.3. Active stress response and active contraction

The active part of the free energy function (9) is formulated through a transversely isotropic function

$$\hat{\Psi}^{\mathrm{a}}(\boldsymbol{g};\boldsymbol{F}^{\mathrm{e}},\boldsymbol{M}) = \tfrac{1}{2}\,\eta(I^{\mathrm{e}}_{4\mathrm{m}}-1)^2 \tag{21}$$

in terms of the active modulus η and the invariant $I^{\mathrm{e}}_{4\mathrm{m}} := \boldsymbol{g} : \boldsymbol{m}^{\mathrm{e}}$ with $\boldsymbol{m}^{\mathrm{e}} := \boldsymbol{F}^{\mathrm{e}}\boldsymbol{M}\boldsymbol{F}^{\mathrm{e}T}$. The active part of the Kirchhoff stress tensor (10) is obtained as

$$\hat{\boldsymbol{\tau}}^{\mathrm{a}}(\boldsymbol{g};\boldsymbol{F}^{\mathrm{e}},\boldsymbol{M}) = 2\,\eta(I^{\mathrm{e}}_{4\mathrm{m}}-1)\boldsymbol{m}^{\mathrm{e}}\,. \tag{22}$$

In order to calculate the active stress tensor $\hat{\boldsymbol{\tau}}^{\mathrm{a}}$, the elastic part of the deformation gradient, which depends on the active part of the deformation gradient must be known. We assume that $\boldsymbol{F}^{\mathrm{a}}$ implicitly depends on the transmembrane potential through the normalized calcium concentration $\bar{c}$ $(23)_1$ and the elastic part of the deformation gradient is expressed through the relation $\boldsymbol{F}^{\mathrm{e}} = \boldsymbol{F}\boldsymbol{F}^{\mathrm{a}-1}$ $(23)_2$. Here, we assume transversely isotropic contraction through

$$\boldsymbol{F}^{\mathrm{a}} = \boldsymbol{1} + (\hat{\lambda}^{\mathrm{a}}(\bar{c})-1)\boldsymbol{M} \quad \text{and} \quad \boldsymbol{F}^{\mathrm{e}} = \boldsymbol{F} - (1-\hat{\lambda}^{\mathrm{a}-1})\boldsymbol{F}\boldsymbol{f}_0\otimes\boldsymbol{f}_0\,. \tag{23}$$

As the myocytes get excited, calcium is released from the sarcoplasmic reticulum into the cytosol, resulting in the contraction of the myocytes. Therefore, the active stretch $\hat{\lambda}^{\mathrm{a}}$ depends on the normalized calcium concentration $\bar{c}$ by the following relationships

$$\hat{\lambda}^{\mathrm{a}}(\bar{c}) = \frac{\xi}{1+f(\bar{c})(\xi-1)}\,\lambda^{\mathrm{a}}_{\mathrm{max}} \quad \text{with} \quad f(\bar{c}) := \frac{1}{2}+\frac{1}{\pi}\arctan(\beta\ln\bar{c}) \quad \text{and} \quad \xi := \frac{f(\bar{c}_0)-1}{f(\bar{c}_0)-\lambda^{\mathrm{a}}_{\mathrm{max}}} \tag{24}$$

where the parameter $\lambda^{\mathrm{a}}_{\mathrm{max}}$ controls the amount of maximum contraction.

3.4. Spatial potential flux

The spatial potential flux $\hat{\boldsymbol{q}}$ has already been introduced in (11) in terms of the conduction tensor $\boldsymbol{D}$ and the potential gradient $\nabla_x\Phi$. In our model, we decompose the second order conduction tensor $\boldsymbol{D}$ into isotropic and anisotropic parts

$$\boldsymbol{D} = d_{\mathrm{iso}}\;\boldsymbol{g}^{-1} + d_{\mathrm{ani}}\;\boldsymbol{m} \tag{25}$$

where d_{iso} and d_{ani} are the scalar conduction coefficients.

3.5. Ventricular pressures

For the three phases of a cardiac cycle, isovolumetric contraction, isovolumetric relaxation and the filling, the left ventricular pressure p_{lv} is modeled by using the Signorini model[31]

$$p_{\mathrm{lv}} := \hat{p}_0 + (\hat{p}_\infty - \hat{p}_0)\,\exp[-\exp(-\chi\tilde{q})] \tag{26}$$

in terms of the normalized flow $\tilde{q} := q - \bar{q}$. Here, q denotes the flow from the left ventricle and is defined as the negative rate of the left ventricular volume change $q := -\dot{V}_{\mathrm{lv}}$. The coefficients $\hat{p}_0$ and $\hat{p}_\infty$ are functions of flow and defined as

$$\hat{p}_0(\tilde{q}) := p_{\mathrm{at}} + m_{\mathrm{at}}\,\tilde{q} \quad \text{and} \quad \hat{p}_\infty(\tilde{q}) := p_{\mathrm{ar}} + m_{\mathrm{ar}}\,\tilde{q} \tag{27}$$

in terms of the atrial pressure p_{at}, the arterial pressure p_{ar}, and the resistance constants m_{at} and m_{ar}. For the evolution of the left ventricular pressure p_{lv} during the ejection phase, we employ the following three-element Windkessel model

$$\dot{p}_{\mathrm{lv}} := \frac{1}{C_{\mathrm{ap}}}(1+\frac{R_{\mathrm{c}}}{R_{\mathrm{p}}})q + R_{\mathrm{c}}\,\dot{q} - \frac{p_{\mathrm{lv}}}{C_{\mathrm{ap}}R_{\mathrm{p}}} \tag{28}$$

in terms of the parameters $R_{\mathrm{c}}, R_{\mathrm{p}}$, and C_{ap} controlling the resistance and compliance characteristics of the hemodynamical system. The right ventricular pressure p_{rv} is assigned to be one-fifth of the left ventricular pressure due to the structural differences. The material parameters of the specified model are introduced in Table 1.

Table 1. Values of the material parameters used for the normal heart

Stress response	$a_1 = 0.496\,\mathrm{kPa}$, $a_{\mathrm{n}} = 3.283\,\mathrm{kPa}$, $a_{\mathrm{k}} = 0.662\,\mathrm{kPa}$, $b_1 = 7.209\,[-]$, $b_{\mathrm{n}} = 11.176\,[-]$, $b_{\mathrm{k}} = 9.466\,[-]$, $\eta = 100\,\mathrm{kPa}$
Active Contraction	$q = 0.1\,[-], k = 0.07\,[-] \beta = 3\,[-], \lambda^{\mathrm{a}}_{\mathrm{max}} = 0.4\,[-]$
Excitation	$\alpha = 0.01\,[-]$, $b = 0.15\,[-]$, $c = 8\,[-], \gamma = 0.002\,[-]$, $\mu_1 = 0.2\,[-]$, $\mu_2 = 0.3\,[-]$
Conduction	$d_{\mathrm{iso}} = 1\ \mathrm{mm}^2/\mathrm{ms}$, $d_{\mathrm{ani}} = 0.1\ \mathrm{mm}^2/\mathrm{ms}$
Pressure Evolution	$\bar{q} = 228\ \mathrm{mm}^3/\mathrm{s}$, $\chi = 1\ \mathrm{ms}/\mathrm{mm}^3$, $p_{\mathrm{at}} = 20\ \mathrm{mmHg}$, $p_{\mathrm{ar}} = 80\ \mathrm{mmHg}$,
(Signorini)	$m_{\mathrm{at}} = 5 \cdot 10^{-3}\ \mathrm{mmHg} \cdot \mathrm{ms}/\mathrm{mm}^3$, $m_{\mathrm{ar}} = 8 \cdot 10^{-2}\ \mathrm{mmHg} \cdot \mathrm{ms}/\mathrm{mm}^3$
Pressure Evolution	$C_{\mathrm{ap}} = 950\ \mathrm{mm}^3/\mathrm{mmHg}$, $R_{\mathrm{c}} = 10^{-3}\ \mathrm{mmHg} \cdot \mathrm{ms}/\mathrm{mm}^3$, $R_{\mathrm{p}} = 1\ \mathrm{mmHg} \cdot \mathrm{ms}/\mathrm{mm}^3$
(Windkessel)	

4. Modeling of myocardial infarction

Myocardial infarction (MI) is one of the leading causes of heart failure. The main reason of MI is the blockage of the blood flow to a part of myocardium, resulting in a lack of oxygen and nutrients necessary for the vital functions of the cardiac cells. If not treated immediately, the contractility of the infarcted region decreases and it becomes stiffer. Therefore, it cannot contribute to the conduction of the electrical signals and the pumping function of the heart anymore. In case of MI, the expected clinical findings on the PV curves are the deviations of the hemodynamic parameters, such as stroke volume (SV), end-diastolic pressure-volume relationship (EDPVR), and end-systolic pressure-volume relationship (ESPVR). These are the indications that the pumping ability of the heart decreases[32].

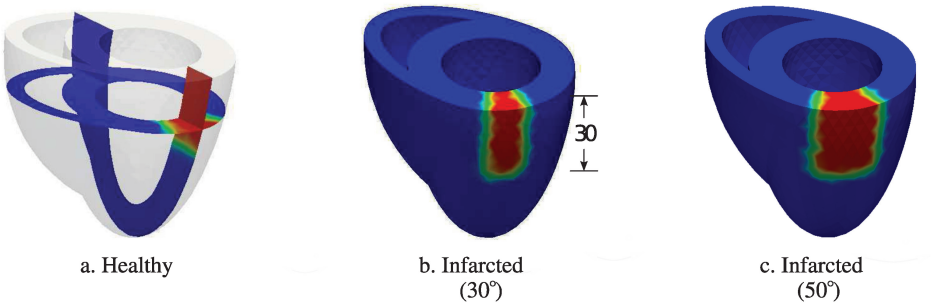

Fig. 3. The locations of the lateral and longitudinal cross-sectional slices, used to generate the snapshots in Figure 4. a) The positions and dimensions of the infarcted regions. Two sizes of infarction have been considered. b) The smaller infarction (30°) extends from θ=120° to θ=150° and c) the large one (50°) is situated between θ=110° and θ=160°. The height of both measures 30 mm.

In this study, we consider two models of infarcted heart with varying sizes of infarcted regions to investigate the relation between the size of the infarction and the change in the electromechanical activity. In Figure 3b and Figure 3c, the infarcted regions are shown in red, while the blue regions represent the healthy myocardium. In the heart with a smaller infarcted region (30°), Figure 3b, the infarction extends from θ=120° to θ=150°. In the heart with a larger

infarction (50°), Figure 3c, the infarcted region is situated between θ=110° and θ=160°. The height of infarction in the both models measures 30 mm.

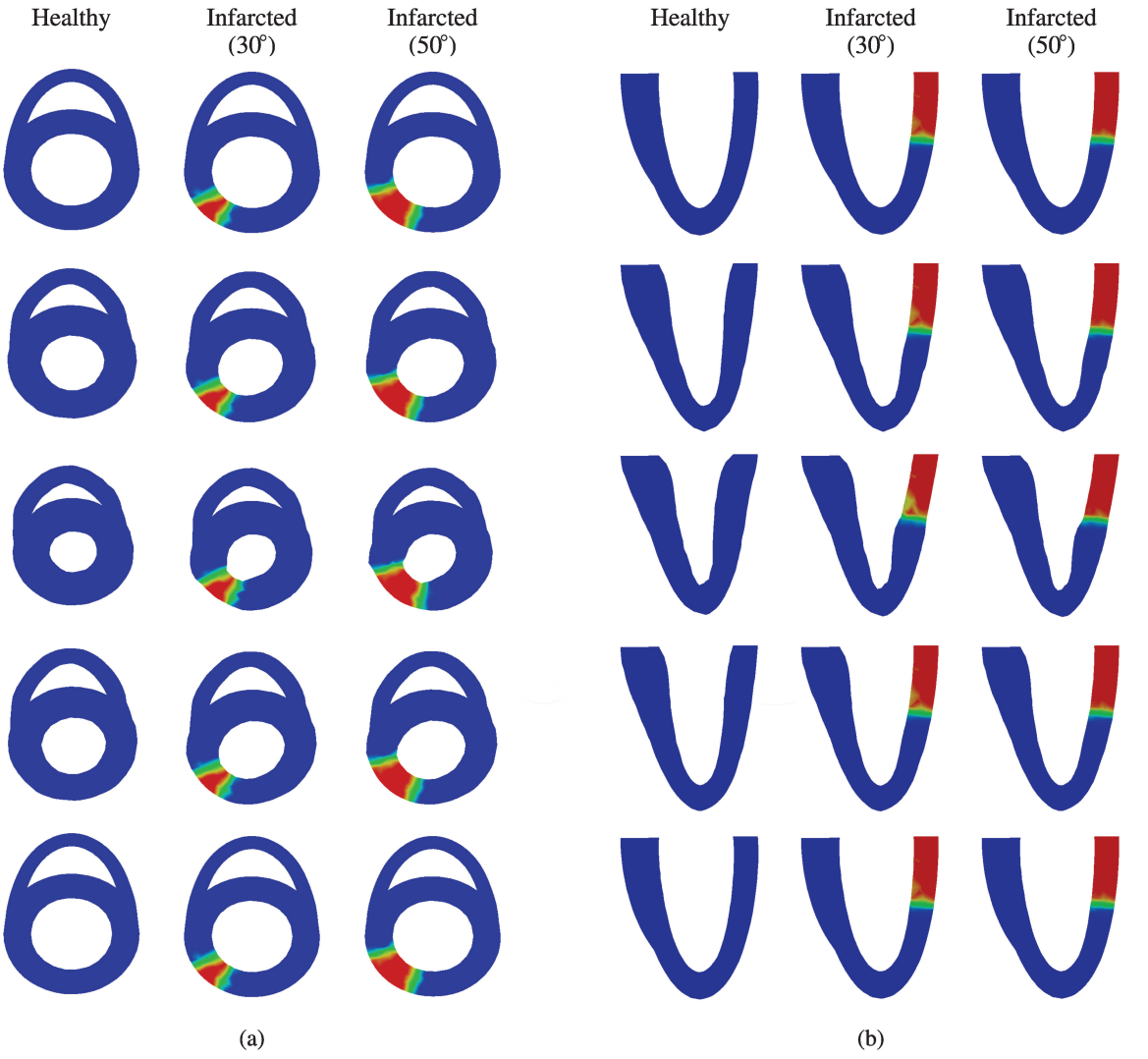

Fig. 4. The snapshots of the lateral (a) and longitudinal (b) slices at different phases of the cardiac cycle are generated by the electromechanical finite element analyses of the heart. First columns in (a) and (b) stand for the healthy heart while the infarcted hearts with 30° and 50° sizes of infarction are shown in the second and third columns in (a) and (b), respectively. The lateral cross-section is located at z=20 mm and the longitudinal cross-section is positioned at θ=135° as depicted in Figure 3a.

The infarcted tissue is modeled by changing some of the material parameters to make the scar tissue stiffer. Therefore, the bulk modulus is magnified by ten, the isotropic modulus is assigned to be $a_1 = 496$ kPa, and we set $\lambda^{\mathrm{a}}_{\mathrm{max}} = 1$. The electromechanical response of the heart is investigated through the electromechanical analysis with the healthy and infarcted heart models with 30° and 50° sizes of infarction. In order to appreciate the decrease in the contractility of the infarcted region, lateral and longitudinal cross-sectional slices taken at z=20 mm and θ=135° are introduced in Figure 4a and Figure 4b, respectively. Here, the first columns of the lateral and longitudinal slices depicts the snapshots of the normal heart, while the second and the third ones represent the infarcted hearts with 30° and 50° sizes of infarction, respectively. As we compare the cross-sectional snapshots generated for the healthy and the infarcted

hearts models, the signs of the decreased overall pumping efficiency, the reduction in contraction and wall thickening are clearly observed. Moreover, the fairly sharp strain gradients observed at the interface between the healthy and infarcted tissue at end-systole (third row in Figure 4) implies the stress concentrations and excessive deformations in the neighborhood of infarction.

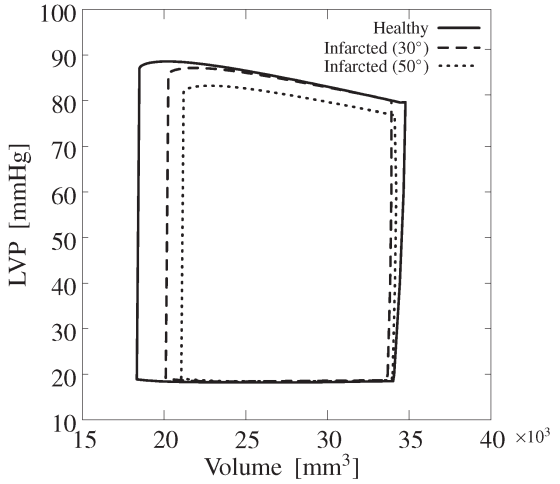

Fig. 5. Left ventricular pressure-volume curves of the generic heart model for healthy and infarcted cases.

In addition to the cross-sectional snapshots, the PV curves are generated for the infarcted hearts in comparison with the PV curve for the healthy heart (Figure 5). To model the ventricular pressure during the ejection phase, the value of the switch flow parameter is modified to capture the steep pressure changes [29]. When the PV curves are compared, we observe that ESPVR becomes more compliant and the ventricular pressure takes lower values during the ejection phase as the infarction gets larger. Moreover, the reduction in SV indicates the decrease in the pumping efficiency of the heart as the infarcted region grows.

5. Concluding remarks

In this contribution, the myocardial infarction has been incorporated into the computational heart model. The coupled problem of cardiac electromechanics has been formulated in the Eulerian setting through the balance of linear momentum and the excitation equations. The specific constitutive equations are introduced to account for the coupled behavior of the heart model through the novel generalized Hill model [19,20] which is an extension of the classical Hill model [33,34]. Utilization of the active-strain and the active-stress based approaches together allows us to combine the advantages of these two methods. In order to model the ventricular pressure evolution, Windkessel-based models are incorporated into the formulation. We employed the computational heart model to investigate the electro-mechanical behavior of the heart for the healthy and infarcted cases, modifying the contractile and mechanical properties of the heart. The performance of our model is illustrated by the generation of the PV curves and shown to resemble the clinical findings, reported in medical literature.

Acknowledgements

This study was supported by the European Union Seventh Framework Programme (FP7/2007-2013) under Grant PCIG09-GA-2011-294161.

References

1. Go, A.S., Mozaffarian, D., Roger, V.L., Benjamin, E.J., Berry, J.D., Borden, W.B., et al. Executive summary: Heart disease and stroke statistics2013 update: A report from the American Heart Association. *Circulation* 2013;**127**:143–152.
2. Gertsch, M.. *The ECG: A Two-Step Approach to Diagnosis*. Springer Science & Business Media; 2003. ISBN 9783540008699.
3. Klabunde, R.E.. *Cardiovascular Physiology Concepts*. Lippincott Williams & Wilkins; 2011.
4. Kerckhoffs, R., Healy, S., Usyk, T., McCulloch, A.. Computational methods for cardiac electromechanics. *Proceedings of the IEEE* 2006; **94**(4):769–783.
5. Dal, H., Göktepe, S., Kaliske, M., Kuhl, E.. A fully implicit finite element method for bidomain models of cardiac electrophysiology. *Computer Methods in Biomechanics and Biomedical Engineering* 2012;**15**(6):645–656.
6. Kerckhoffs, R.C.P., Omens, J.H., McCulloch, A.D.. Mechanical discoordination increases continuously after the onset of left bundle branch block despite constant electrical dyssynchrony in a computational model of cardiac electromechanics and growth. *Europace* 2012;**14 Suppl 5**:v65–v72.
7. Rantner, L.J., Tice, B.M., Trayanova, N.A.. Terminating ventricular tachyarrhythmias using far-field low-voltage stimuli: mechanisms and delivery protocols. *Heart rhythm: the official journal of the Heart Rhythm Society* 2013;**10**:1209–1217.
8. Roberts, B.N., Yang, P.C., Behrens, S.B., Moreno, J.D., Clancy, C.E.. Computational approaches to understand cardiac electrophysiology and arrhythmias. *American Journal of Physiology - Heart and Circulatory Physiology* 2012;**303**:H766–H783.
9. Cherubini, C., Filippi, S., Nardinocchi, P., Teresi, L.. An electromechanical model of cardiac tissue: Constitutive issues and electrophysiological effects. *Progress in Biophysics and Molecular Biology* 2008;**97**(23):562–573.
10. Nobile, F., Quarteroni, A., RuizBaier, R.. An active strain electromechanical model for cardiac tissue. *International Journal for Numerical Methods in Biomedical Engineering* 2012;**28**(1):52–71.
11. Rossi, S., Ruiz-Baier, R., Pavarino, L.F., Quarteroni, A.. Orthotropic active strain models for the numerical simulation of cardiac biomechanics. *International Journal for Numerical Methods in Biomedical Engineering* 2012;**28**(6-7):761–788.
12. Stålhand, J., Klarbring, A., Holzapfel, G.. A mechanochemical 3D continuum model for smooth muscle contraction under finite strains. *Journal of Theoretical Biology* 2011;**268**(1):120–130.
13. Keldermann, R., Nash, M., Panfilov, A.. Pacemakers in a Reaction-Diffusion mechanics system. *Journal of Statistical Physics* 2007; **128**(1):375–392.
14. Niederer, S.A., Smith, N.P.. An improved numerical method for strong coupling of excitation and contraction models in the heart. *Progress in Biophysics and Molecular Biology* 2008;**96**(1-3):90–111.
15. Göktepe, S., Kuhl, E.. Electromechanics of the heart: a unified approach to the strongly coupled excitation-contraction problem. *Computational Mechanics* 2010;**45**(2-3):227–243.
16. Lafortune, P., Ars, R., Vázquez, M., Houzeaux, G.. Coupled electromechanical model of the heart: Parallel finite element formulation. *International Journal for Numerical Methods in Biomedical Engineering* 2012;**28**:72–86.
17. Eriksson, T.S.E., Prassl, A.J., Plank, G., Holzapfel, G.A.. Influence of myocardial fiber/sheet orientations on left ventricular mechanical contraction. *Mathematics and Mechanics of Solids* 2013;doi:10.1177/1081286513485779; in press.
18. Eriksson, T.S.E., Prassl, A.J., Plank, G., Holzapfel, G.A.. Modeling the dispersion in electromechanically coupled myocardium. *International Journal for Numerical Methods in Biomedical Engineering* 2013;doi:10.1002/cnm.2575; in press.
19. Göktepe, S., Menzel, A., Kuhl, E.. Micro-structurally based kinematic approaches to electromechanics of the heart. In: Holzapfel, G.A., Kuhl, E., editors. *Computer models in Biomechanics. From Nano to Macro*; chap. 13. Springer Science+Business Media Dordrecht; 2013, p. 175–187.
20. Göktepe, S., Menzel, A., Kuhl, E.. The generalized hill model: A kinematic approach towards active muscle contraction 2013;Submitted for publication.
21. Aliev, R.R., Panfilov, A.V.. A simple two-variable model of cardiac excitation. *Chaos, Solitons and Fractals* 1996;**7**(3):293–301.
22. Göktepe, S., Kuhl, E.. Computational modeling of cardiac electrophysiology: A novel finite element approach. *International Journal for Numerical Methods in Engineering* 2009;**79**:156–178.
23. Keener, J.P., Sneyd, J.. *Mathematical Physiology*. New York: Springer; 1998.
24. Fitzhugh, R.. Impulses and physiological states in theoretical models of nerve induction. *Biophysical Journal* 1961;**1**:455–466.
25. Nagumo, J., Arimoto, S., Yoshizawa, S.. An active pulse transmission line simulating nerve axon. *Proceedings of the IRE* 1962; **50**(10):2061–2070.
26. Ambrosi, D., Arioli, G., Nobile, F., Quarteroni, A.. Electromechanical coupling in cardiac dynamics: The active strain approach. *SIAM Journal on Applied Mathematics* 2011;**71**(2):605–621.
27. Ask, A., Menzel, A., Ristinmaa, M.. Electrostriction in electro-viscoelastic polymers. *Mechanics of Materials* 2012;**50**:9 – 21.
28. Ask, A., Menzel, A., Ristinmaa, M.. Phenomenological modeling of viscous electrostrictive polymers. *International Journal of Non-Linear Mechanics* 2012;**47**(2):156 – 165.
29. Berberoğlu, E., Solmaz, H.O., Göktepe, S.. Computational approaches to coupled cardiac electromechanics incorporating dysfunctional cases. *European Journal of Mechanics A/ Solids* 2014;DOI: 10.1016/j.euromechsol.2014.02.021.
30. Holzapfel, G.A., Ogden, R.W.. Constitutive modelling of passive myocardium: a structurally based framework for material characterization. *Philosophical Transactions Series A, Mathematical, Physical, and Engineering Sciences* 2009;**367**(1902):3445–3475.
31. Sainte-Marie, J., Chapelle, D., Cimrman, R., Sorine, M.. Modeling and estimation of the cardiac electromechanical activity. *Computers & Structures* 2006;**84**(28):1743–1759.
32. Katz, A.M.. *Physiology of the Heart*. Philadelphia, PA: Wolters Kluwer Health/Lippincott Williams & Wilkins Health; 2011.
33. Hill, A.V.. The heat of shortening and the dynamic constants of muscle. *Proceedings of the Royal Society of London Series B - Biological Sciences* 1938;**126**(843):136–195.
34. Hill, A.V.. *First and Last Experiments in Muscle Mechanics*. Cambridge University Press; 1970.